RESPONSE OF A REINFORCED CONCRETE EMBEDDED PILE UNDER LATERAL LOADING. II: NUMERICAL STUDIES

C. Rha, E. Taciroglu, J.W. Wallace, E. Ahlberg, J.P. Stewart
University of California, Los Angeles, CA, 90095-1593, USA.

INTRODUCTION

A cast-in-drilled-hole, 2 ft (~61 cm) diameter reinforced concrete pile (shaft) has been tested in the field. The shaft is embedded in the soil by 25 ft (7.62 m), and extends above the ground line by 13.4ft. It is reinforced with eight #9 longitudinal bars ($\rho = A_s / A_g = 0.0177$) and with #6 hoops at four-inch spacing ($\rho_s = 4A_{sp} /(sD_c) = 0.0226$), where, A_s, A_{sp} are the cross-sectional areas of longitudinal and spiral bars, respectively, A_g is the gross cross-sectional area of the shaft, s is the core diameter, and D_c is the (out-to-out) diameter of the spiral. The shaft-head is free to rotate and is subjected to lateral loading. Further details on the specimen, instrumentation, and loads are provided in the companion paper (Ahlberg et al., 2005).

Here, we focus on numerical simulations of the response of the pile and of the surrounding soil layers using several distinct methods. One objective of these simulations was to predict the field-response in order to plan the loading protocols and the instrumentation layout for the tests. Another key objective was to provide a series of "blind" (pre-test) predictions that could then be compared to the observed response for the various analytical approaches considered. Finally, we seek to identify the cause of misfits between pre-test predictions and test results. Three approaches are used in developing the numerical models; namely, (*i*) the three-dimensional finite element method, (*ii*) the macroelement method by Taciroglu et al. (2003, 2004), and (*iii*) the strain-wedge method by Ashour et al. (2002). The computer codes used for each simulation, respectively, are ABAQUS (a proprietary finite element analysis package), FrameLab developed at UCLA, and SWM (Ashour, 2002). A variety of other analysis packages (OpenSees, Biax, etc.) are also utilized for minor validation and verification tasks. The models developed here share common features, such as a subset of the material response parameters, descriptions of the specimen geometry, and the loading; yet they differ in the way these attributes are implemented. The descriptions of the models are presented below, followed by the simulation results and comparisons with field-test data. It should be noted that the presented results are preliminary and are limited to pushover analyses; cyclic loading results are deferred to a subsequent publication.

THREE-DIMENSIONAL FINITE ELEMENT MODEL

The three-dimensional finite element model has a circularly symmetric mesh and consists of two major parts, namely, the mesh for the reinforced concrete shaft and that for the soil layers, as illustrated in Figure 1. The total depth and the diameter of the model are 48 ft (14.63 m) and 22 ft (6.71 m), respectively. The base-soil domain (i.e., soil below the shaft) is divided into 5 layers of

varying thicknesses. The upper-soil domain (i.e., soil adjacent to the shaft) is modeled with 16 layers, thus, a total of 21 soil layers are used in the vertical direction. The upper-soil domain is divided into eight 1 ft (30.48 cm)-thick layers (where highly nonlinear soil behavior is expected) from the top, while the rest—from 8 ft (2.44 m) to 25 ft (7.62 m)—is divided into another eight uniform thickness (~2 ft or ~0.61 m) layers. The extent of the soil domain in the radial direction is chosen to be 11 times the shaft diameter (i.e., 22 ft or 6.71 m). This choice was based on several parametric studies with the mesh diameter, and it was found that the use of a larger mesh diameter does not significantly affect the near-field soil or the shaft response.

The soil domain is divided into 5 segments with varying lengths along the radial direction. The soil surrounding the shaft is modeled using 8-node brick elements (C3D8 in ABAQUS element library) and the soil below the shaft is modeled using 6-node triangular prism elements (C3D6 in ABAQUS) as illustrated in Figure 1. Eight-node infinite elements with radial foci are used at the lateral limits of the model to simulate far field behavior (CIN3D8 in ABAQUS). The bottom nodes of the finite element mesh are fixed in the vertical direction. As there are no directly applied vertical loads, this is deemed as a reasonable assumption for the sake of computational efficiency. As such, a total of 1840 finite elements (1760 C3D8's and 80 C3D6's) and 336 infinite elements (CIN3D8's) are used to model soil domain.

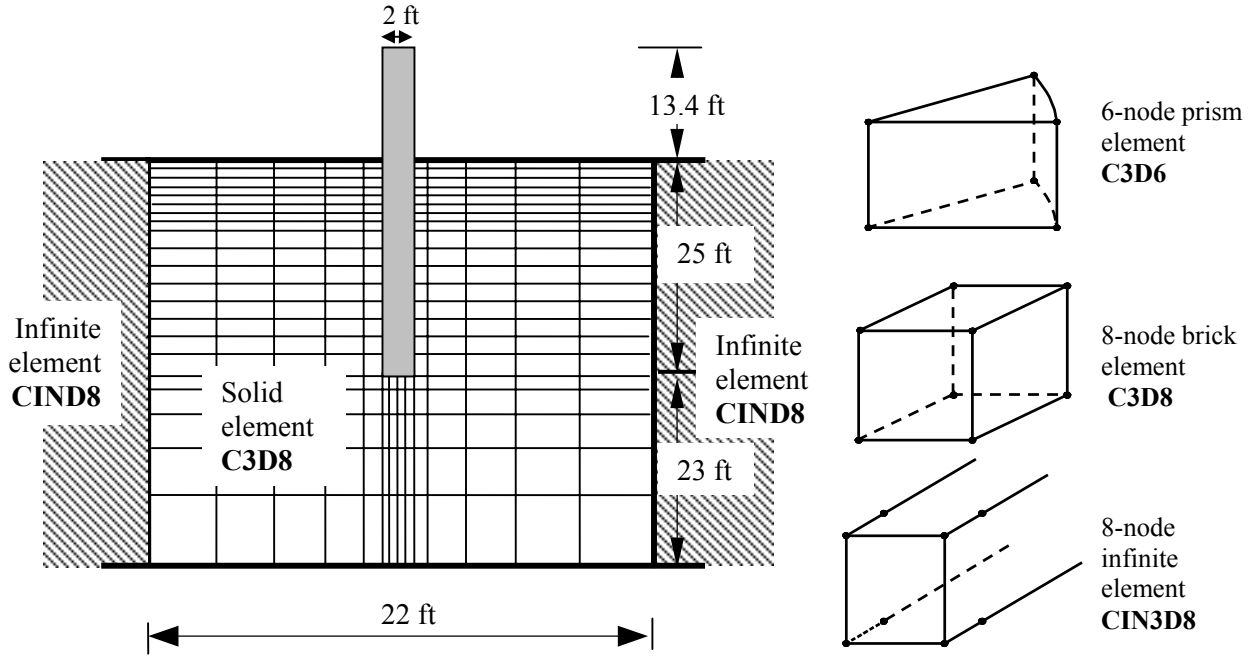

Figure 1. 3D finite element model: Geometry (left), and ABAQUS elements used (right).

The reinforced concrete shaft is modeled with solid and truss elements. Truss elements are used for modeling the steel reinforcement; and two different types of solid elements are used for modeling the concrete, as illustrated in Figure 2. The cross-section of the shaft is divided into 16 solid finite elements with 8 elements representing concrete inside the hoop reinforcement, and another 8 for the outer region. The inner and the outer solid elements are 15-node (quadratic) triangular prisms (C3D15 in ABAQUS), and 20-node quadratic bricks (C3D20 in ABAQUS), respectively. The inner part of the cross-section forms the confined-concrete region that is surrounded by the hoops, while the outer part forms the unconfined-concrete region. The

longitudinal steel bars are modeled using 3-node quadratic truss elements (T3D3), which are anchored at the interface points of the C3D15's and the C3D20's as illustrated Figure 2. The nodal spacing of the finite elements for the shaft below the ground line is identical with those of the soil layers described earlier. The upper portion of the shaft (above the ground-line) is divided into finite elements with nodal spacing that ranges from 1 ft (30.48 cm) to 1.66 ft (50.6 cm) or larger (i.e., up to 5 ft or 152.4 cm) above the ground line. In total, the shaft is divided into 26 segments along the length, and each segment contains 16 solid and 8 truss elements. Therefore the shaft is modeled using a total of 624 finite elements (208 each of C3D15's, C3D20's, and T3D3's)

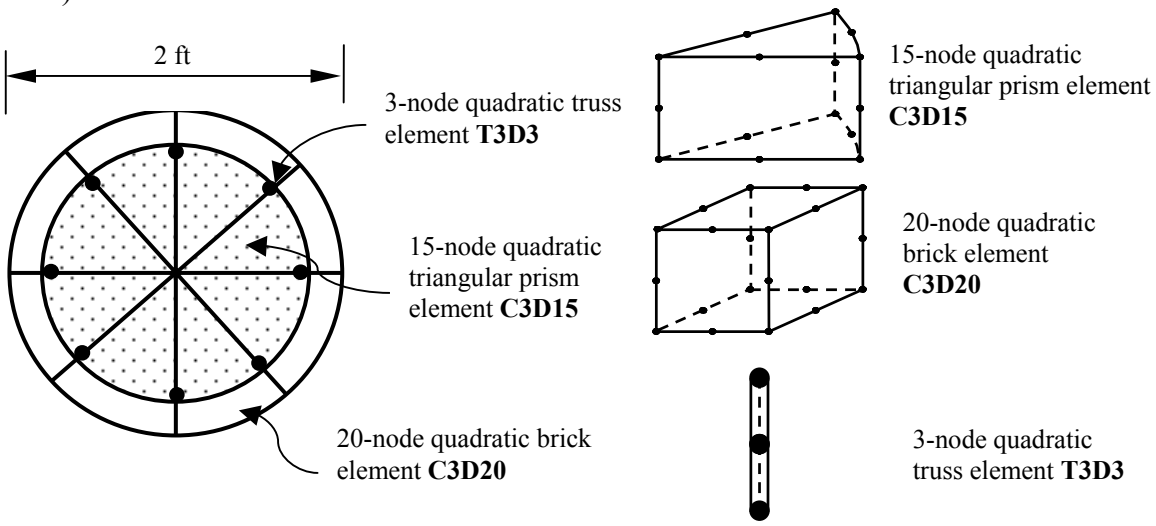

Figure 2. Concrete shaft model for FEM: Shaft section (left), finite elements used (right).

The interface between the soil and the shaft elements is modeled using the "contact pairs" option in ABAQUS. The soil and the shaft surfaces are defined as "slave," and "master" surfaces, respectively, because the shaft is stiffer than the soil layers. The solid elements for the shaft (i.e., all of C3D20's and C3D15's) are converted automatically to appropriate variable-node element types that are brick elements with 21 to 27 nodes (C3D27's) and triangular prism elements with 15 to 18 nodes (C3D15V's) if they are adjacent to a slave surface in a contact pair.

Material Properties for the Finite Element Model

The soil properties are based on an earlier investigation of the test site (Janoyan et al., 2001). The Mohr-Coulomb model is used to describe the soil behavior, and thus, yielding occurs when shear stress on any plane in the material reaches a certain limit value that depends linearly on the normal stress on the same plane. The complete set of material parameters used for defining the Mohr-Coulomb model in ABAQUS and their assigned values for this particular simulation are as follows:

- Unit weight, γ =125 pcf = 2000 kg/m^3,
- Poisson's ratio, ν = 0.3 (drained), ν = 0.46 (undrained),
- Cohesion (c), Internal friction and dilation angles (ϕ, ψ):

  -48 ft (-14.6m)$\leq z \leq$ -25 ft (-7.6m), c = 4700 psf = 225 kPa, $\phi = \psi = 1^o$ (clay, undrained),

  -25 ft $\leq z \leq$ -22 ft (-6.7 m), c = 150 psf = 7.18 kPa, $\phi = \psi = 38^o$ (sand, drained),

  -22 ft $\leq z \leq$ 0 ft, c = 3900 psf = 187 kPa, $\phi = \psi = 1^o$ (clay, undrained),

- Young's Modulus, $E = 7\text{x}10^6$ psf = 335.2 MPa (far field), $E = 4\text{x}10^6$ psf = 191.5 MPa (within one diameter distance of the shaft; reduced value is used to take the excavation effects into account).

The uniaxial compressive strength for concrete is assumed to be 4 ksi (27.6 MPa). The concrete stress-strain behavior inside the spiral reinforcement is modeled using the modified Kent-Park model by Park et al. (1982), with a minor revision to take into account the circular geometry of the cross-section. Adopting the convention that compression is positive, the stress and corresponding tangent moduli in the ascending and descending regions of the concrete constitutive model can be described as

$$\begin{cases} \sigma_c = Kf_c^{'}\left[2\left(\dfrac{\varepsilon_c}{\varepsilon_0}\right)-\left(\dfrac{\varepsilon_c}{\varepsilon_0}\right)^2\right] \text{ and } E_t = \dfrac{2Kf_c^{'}}{\varepsilon_0}\left(1-\dfrac{\varepsilon_c}{\varepsilon_0}\right) \\ \sigma_c = Kf_c^{'}\left[1-Z(\varepsilon_c-\varepsilon_0)\right] \geq 0.2Kf_c^{'} \text{ and } E_t = -ZKf_c^{'} \ (=0 \text{ if } \sigma_c \leq 0.2Kf_c^{'}) \end{cases} \tag{1}$$

where ε_0 and ε_{20} are the concrete strain at 100% and 20% of the peak stress, respectively, K is a factor which accounts for the strength increase due to confinement, and Z is the slope of strain softening. These last two parameters are defined as

$$K = 1+\frac{\rho_s f_{yh}}{f_c^{'}},\ \varepsilon_0 = 0.002K,\ \text{ and } \ Z = \frac{1}{2}\left[\frac{3+f_c^{'}}{f_c^{'}-1000}+0.75\rho_s\sqrt{\frac{h^{'}}{s_h}}-\varepsilon_0\right]^{-1} \tag{2}$$

where the yield strength of hoop reinforcement is $f_{yh} = 68$ ksi (469MPa), the ratio of the volume of hoop reinforcement to the volume of the concrete core is $\rho_s = 0.0226$, the width of concrete core is $h' = 20\,\text{in}$ (50.8 cm), and the center-to-center spacing of the hoops is $s_h = 4$ in (10.2 cm). The longitudinal and the transverse reinforcements are Grade-A615 and Grade-A706 steel, respectively. The yield strength of the longitudinal bars is assumed to be 68 ksi (469 MPa), and hardening is considered as defined in Biax (Wallace and Ibrahim, 1996). The Biax constitutive model for steel is approximated with a piecewise linear relationship in ABAQUS.

MACROELEMENT MODEL

The analyses performed with this approach are carried out using a computer code (FrameLab) developed at UCLA. The concrete shaft is modeled using fiber-based beam finite elements and soil response is modeled using macroelements, as illustrated in Figure 3. The FrameLab program was used because it more readily allows for customization of reinforced concrete and soil spring elements than other commercial or academic software such as LPile or OpenSees. FrameLab has been validated against those codes using appropriate benchmark problems (Taciroglu et al., 2004). The FrameLab soil macroelements can incorporate frictional forces and formation of gaps at the soil-pile interface as well as the hysteretic behavior of the soil under cyclic loads.

The cross-section of the shaft consists of steel reinforcement, and confined/unconfined concrete, similar to the three-dimensional finite element model shown in Figure 2. However, in this approach, the shaft is modeled with fibers (Spacone et al., 1996), rather than solid finite elements. The section is divided into 8 unconfined concrete fibers, 24 confined concrete fibers, and 8 numbers of steel fibers as shown in Figure 3. The macroelements for the soil are located at 2 ft spacing (61 cm); thus, there are 13 such elements. Parametric studies indicated that a more refined (i.e., smaller) spacing of macroelements does not significantly affect the computed response. Macroelements consist of a parallel combination of drag, leading-face, and rear-face

subelements as illustrated in Figure 3. The leading and rear-face elements produce elastoplastic response with a specific envelope under compressive loading. These envelope curves are known as "*p-y*" curves, and are usually calibrated with full-scale field tests. Detailed descriptions of the macroelements are provided in Taciroglu et al. (2003, 2005) and in Rha et al. (2004).

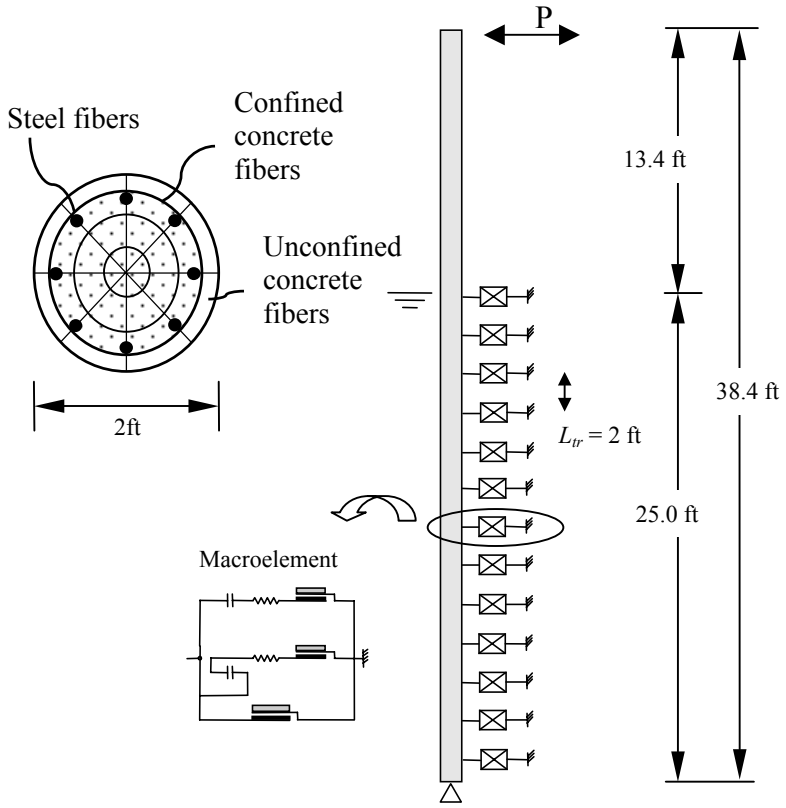

Figure 3. The macroelement model geometry and the cross-section.

Material Properties for the Macroelement Model

For steel fibers, we use the constitutive relationship by Filippou et al. (1983), which is an enhanced version (with isotropic strain hardening) of that by Menegotto and Pinto (1973). The yield strength is assumed to be 68 ksi (469 MPa) with 20% strain hardening. The constitutive relationships for (confined and unconfined) concrete are the cyclic models proposed by Mohd-Yassin (1994) who implemented a cyclic loading capability over the monotonic envelope of the modified Kent-Park model (Park et al., 1982). Since only pushover analysis results are compared in this manuscript, the constitutive relations used for the unconfined/confined concrete fibers are identical to that of the finite element simulations.

Two types of *p-y* curves are used to represent the inelastic soil response: "Standard (or API) *p-y* curves" (API, 1993) and "experimental *p-y* curves." The experimental curves are obtained from an earlier full-scale field-test of a large-diameter (6ft) shaft (Janoyan et al., 2001). The calibration of *p-y* curves for the 2 ft (61 cm) diameter shaft was carried out by scaling down the experimental *p-y* curves of the 6 ft (183 cm) diameter shaft with conversion factors (the ratio of ultimate resistance of soil for the 2 ft diameter shaft over that of the 6 ft diameter shaft based on API formulation). For the formulation of the calibrated (experimental) *p-y* curves, the same exponential form defined in API (1993) has been employed with some minor modifications. The

API curves are parameterized using the undrained shear strength (c), unit weight of the soil (γ), shaft diameter (D), an empirical constant (J), strain at one-half the maximum stress (ε_c) and depth (z), and those same parameters are used to describe the experimental curves. This functional form is described by,

$$p/p_u = \left(y/y_{50}\right)^n \le 1.0 \tag{3}$$

with $p_u = N \cdot c \cdot D$, and $N = 30/z_f + \gamma z/c + Jz/D \ge z_f/6$. For the experimental curve, we have

$$n = 3/2, \quad y_{50} = \left[8.5 + z_f\left(1 - z_f\right)/12\right]\varepsilon_{50} D \ge 0.35\varepsilon_{50} D, \quad J = 5.6 - z_f\left(1 - z_f\right)/20 \ge 0.1 \tag{4}$$

where $z_f \ge 3$ ft (92 cm) denotes the depth. On the other hand, for the API curve, we have

$$n = 1/2, \quad y_{50} = 2.5\varepsilon_{50} D, \quad J = 0.25 \tag{5}$$

The parameters that have common values for both curves are γ = 125 pcf, c = 3900 psf, and ε_{50} = 0.007. The experimental p-y curves for the 6 ft shaft and the scaled p-y curves for the 2 ft shaft are displayed in Figure 4.

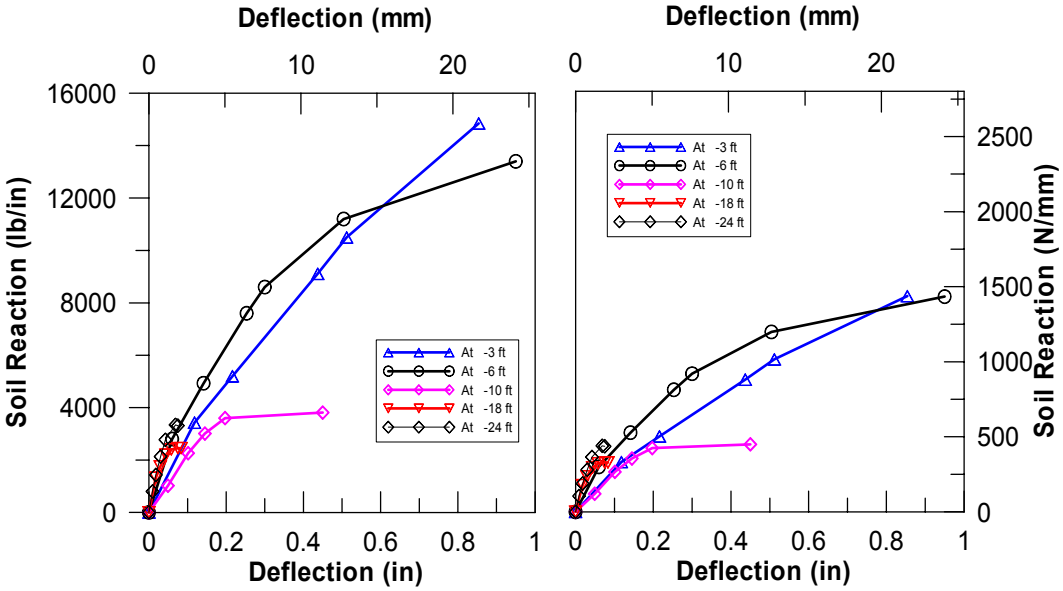

Figure 4. Curve-fits to experimental *p-y* curves of Janoyan et al. (2001) for 6 ft shaft (left), adjusted to 2 ft shaft (right).

STRAIN WEDGE MODEL

The strain wedge model by Norris (1986), later updated by Ashour et al. (2002), provides an alternative analysis method for soil-pile interaction behavior, in which soil failure is assumed to occur on a prescribed failure plane. For the simulations in this study, the SWM computer program (developed by Ashour) is used. The strain-wedge model of the test specimen consists of a single segment of nonlinear concrete shaft and three layers of soil—i.e., 10 ft (3.05 m) of base-soil, 3 ft (0.91 m) of sand, and 22 ft (6.71 m) of clay.

Material Properties for the Strain-Wedge Model

The uniaxial compressive strength of concrete and the yield stress of steel are 4 ksi (27.6 MPa) and 68 ksi (468.8 MPa), as before. Unlike the fiber-based model used in FrameLab, the reinforcement input is based on the steel ratio. The longitudinal and transverse steel ratios for the shaft are chosen to be 0.018 and 0.022, consistent with the FrameLab and ABAQUS models. The strain wedge model requires the following properties from the soil profile: effective unit weight of soil (γ), effective angle of internal friction (φ), axial strain at 50% of stress level (ε_{50}), and undrained shear strength for clay (S_u) in addition to the thickness of each of the soil layers. Therefore, soil properties used in previous models are identical to those used in this model (i.e., γ = 125 pcf, φ = 1° and 38° for clay and sand, S_u =3900 psf, and ε_{50} = 0.007).

A PRELIMINARY COMPARISON OF RESULTS AND CONCLUSIONS

As noted earlier, all of the simulation results in this study are produced with our best estimates of actual material properties, i.e. the material parameters are not tuned to reproduce test results. Figure 5 presents two sets of *preliminary* comparisons of **M**oment vs. **C**urvature (MC), and lateral **L**oad vs. pile-**T**op **D**isplacements (LTD). Although the MC responses of each simulation model are similar (Figure 5, left), they all over-predict the specimen MC. On the other hand, the predicted LTD responses are more variable (Figure 5, right) than the corresponding MC's. Nonetheless, the predicted LTD's are reasonably similar to the specimen LTD. An inspection of the LTD comparisons yields the following observations: (1) macroelement (with the API backbone curve) and FEM simulations predict the ultimate load (capacity) quite well; (2) macroelement (with API backbone curve) and strain-wedge simulations predict the LTD response reasonably well; (3) macroelement (with experimental backbone curve) and strain-wedge simulations significantly over- and under-predict the specimen's load capacity, respectively; and finally, (4) the initial stiffness of the pile-soil system is over-predicted by the FEM.

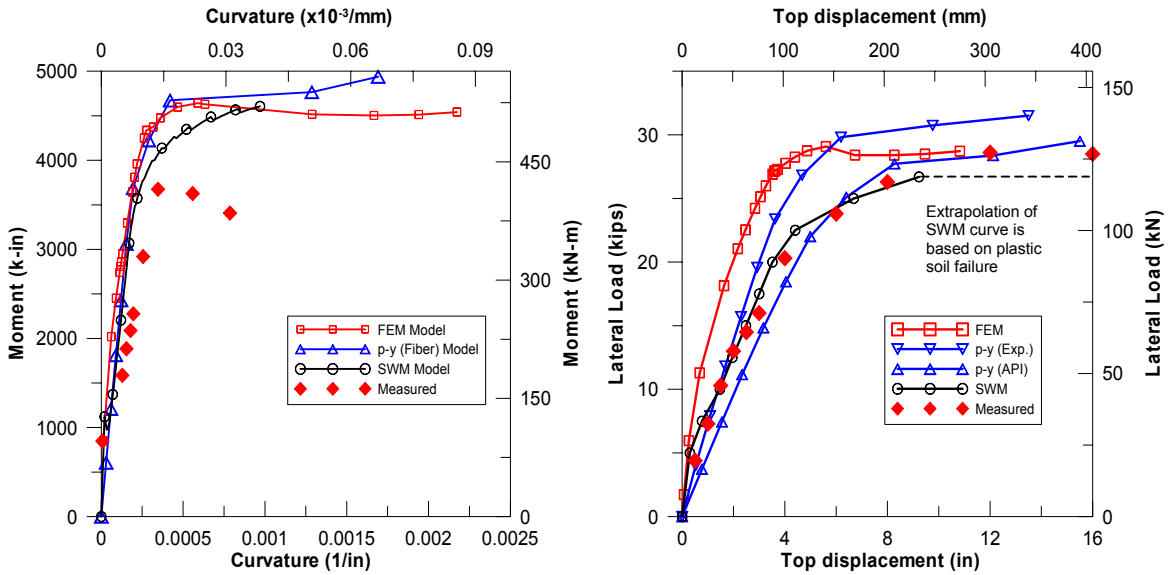

Figure 5. Comparison of moment-curvature relationships, and top displacements versus loads.

Ultimately, these preliminary results will be revisited, and the sensitivity of model predictions with respect to uncertainties in the model parameters will be determined through parametric studies. It is anticipated that, within reasonable ranges of the model parameters, all of the

simulation tools will yield acceptable results for this small/medium-diameter pile. On the other hand, based on the present preliminary results, it is very likely that the use of experimental (2 ft) *p-y* curve, which was scaled down from that of a large-diameter pile test (Janoyan et al. 2001), is the least accurate approach. If this assertion is true, then the implications are that (1) the scaling law that we have used is not correct and must be rectified, and by the same token, (2) *p-y* curves for small-diameter piles (i.e., standard API curves) are not suitable for large-diameter piles. Future studies on existing data and subsequent tests will shed light to these issues.

REFERENCES

ABAQUS, User's Manual (2003). ABAQUS, Inc., Version 6.4.

Ahlberg E, Stewart JP, Wallace JW, Rha C, Taciroglu E (2005). "Response of a reinforced concrete embedded pile under lateral loading. I: Field-testing," *2005 Caltrans Bridge Research Conference*, October 1, 2005, Sacramento CA, Paper 01-505.

American Petroleum Institute (API) (1993). "Recommended Practice for Planning, Designing, and Constructing Fixed Offshore Platforms–Working Stress Design." *20th Ed., API RP2A-WSD*, Washington, D.C.

Ashour M, Norris G, Pilling P (2002). "Strain wedge model capability of analyzing behavior of laterally loaded isolated piles, drilled shafts, and pile groups." *Journal of Bridge Engineering*, ASCE, 7(4), 245-254.

Filippou FC, Popov EP, Bertero VV (1983). "Effects of Bond Deterioration on Hysteretic Behavior of Reinforced Concrete Joints." *Rep. No. UCB/EERC-83/19*, Earthquake Engrg. Res. Ctr., University of California, Berkeley, Calif.

Janoyan KP, Stewart JP, Wallace JW (2001). "Test results for full-scale drilled shafts under cyclic lateral loading." *Prog. Report to Caltrans,* UCLA.

Menegotto M, Pinto PE (1973). "Method of analysis for cyclically loaded reinforced concrete plane frames including changes in geometry and non-elastic behavior of elements under combined normal force and bending." *Proc., IABSE Symp. on Resistance and Ultimate Deformability of Struct. Acted on by Well-Defined Repeated Loads*, Lisbon.

Mohd-Yassin MH (1994). "Nonlinear analysis of prestressed concrete structures under monotonic and cyclic loads." *PhD. Thesis*, University of California, Berkeley, California.

Norris GM (1986). ''Theoretically based BEF laterally loaded pile analysis.'' *Proc., 3rd Int. Conf. on Numerical Methods in Offshore Piling*, TECHNIP Ed., Paris, 361–386.

OpenSees, http://opensees.berkeley.edu/OpenSees/developer.html

Park R, Priestley MJ, Gill WD (1982). "Ductility of square-confined concrete columns." *Journal of the Structural Division*, ASCE, 108(ST4), 135-137.

Rha CS, Wallace JW, Taciroglu E (2004). "Analytical modeling of soil-structure interaction for bridge columns." *13th World Conf. on Earthq. Eng.*, Vancouver, B.C. Canada.

Spacone E, Filippou FC, Taucer FF (1996). "Fiber Beam-Column Model for Nonlinear Analysis of R/C Frames: Part I. Formulation." *Earthq. Eng, and Struct. Dyn.,* 25, 711-725.

Taciroglu E, Rha CS, Stewart JP, Wallace JW (2003). "Robust numerical models for cyclic response of columns embedded in soil." *Proc., 16th ASCE Eng. Mech. Conf.*, University of Washington, Seattle.

Taciroglu E, Rha CS, Wallace JW (2004). "A Robust macroelement model for soil-pile interaction under cyclic loads." *Journal of Geotech. and Geoenv. Eng.,* ASCE (submitted).

Wallace JW, Ibrahim YA (1996). Biax for MS Windows.